A General Strategy To Fabricate Simple Polyoxometalate Nanostructures: Electrochemistry-Assisted Laser Ablation in Liquid

Pu Liu, Ying Liang, Xianzhong Lin, Chengxin Wang, and Guowei Yang*

State Key Laboratory of Optoelectronic Materials and Technologies, Institute of Optoelectronic and Functional Composite Materials, Nanotechnology Research Center, School of Physics & Engineering, Sun Yat-sen University, Guangzhou 510275, Guangdong, People's Republic of China

ABSTRACT Polyoxometalate nanostructures have attracted much attention because of significant technical demands in applications such as catalysts, sensors, and smart windows. Therefore, researchers have recently developed many methods for the synthesis of these nanomaterials. However, these techniques have many visible flaws such as high temperatures or high pressure environments, various templates or additives, demanding and complicated synthesis procedures as well as the presence of impurities in the final products. We therefore propose a general strategy for the fabrication of particular polyoxometalate nanostructures by electrochemically assisted laser ablation in liquid (ECLAL). These polyoxometalates are usually simple as they typically contain two metals and are not soluble in water. This approach is a green, simple, and catalyst-free approach under an ambient environment. Apart from these merits, this novel technique allows researchers to choose and design interesting solid targets and to use an electrochemical approach toward the fabrication of polyoxometalate nanostructures for the purpose of fundamental research and for potential applications. Using the synthesis of $Cu_3Mo_2O_9$ nanorods as an example, we substantiate the validity of the proposed strategy. For the fabrication of $Cu_3Mo_2O_9$ nanostructures, we chose molybdenum as a solid target for laser ablation in liquid copper electrodes for the electrochemical reaction and water as a solvent for the ECLAL synthesis. We successfully fabricated $Cu_3(OH)_2(MoO_4)_2$ nanorods with magnetic properties. Interestingly, we obtained well-defined $Cu_3Mo_2O_9$ nanorods by annealing the $Cu_3(OH)_2(MoO_4)_2$ nanostructures at 500 °C. Additionally, the basic physics and chemistry involved in the ECLAL fabrication of nanostructures are discussed.

KEYWORDS: laser ablation in liquid · electrochemistry · fabrication · polyoxometalate nanostructures

Chemically speaking, the polyoxometalates (POMs) are a large family of inorganic compounds, whereas, in general, use POM is a designation for a large range of inorganic materials. These are always polyatomic ion compounds that consist of at least two but usually three or more transition metal oxyanions that are linked together by shared oxygen atoms to form a large, closed three-dimensional framework. Sometimes the transition metal oxyanion framework may enclose one or more heteroatoms, such as phosphorus or silicon, to share neighboring oxygen atoms within the framework. For example, the phosphotungstate anion $[PW_{12}O_{40}]^{3-}$ is a typical polyoxometalate anion. The POMs represent a diverse range of micro- and nanoclusters, which exhibit an unmatched range of physical and chemical properties while they can form novel functional structures. These characteristics have thus attracted critical attention in material science research.[1−3] Recently, some simple POMs (*e.g.*, binary metal oxides containing Mo, W, V, Ta, and a second transition metal such as Cu, Fe, Co, or Ni species) have been studied extensively because of industrial interest in their robust catalytic property in crude oil refining,[4,5] emissive display technology,[6,7] magnetism,[8] sorption,[9] and energy storage.[10] To improve the performance of POMs, researchers have developed several techniques for the synthesis of POM nanostructures.[11−14] However, these methods have some visible flaws such as the synthesis route requiring high temperature or high pressure conditions, the introduction of various templates or additives, and demanding as well as complicated synthetic procedures that result in impurities in the final products *etc*. These factors restrict their application in industry. Therefore, developing a new synthesis for POM nanostructures is becoming urgent.

In this contribution, we propose a general strategy for the fabrication of one kind of POM nanostructure by electrochemically assisted laser ablation in liquid (ECLAL). This kind of POM is usually simple as it typically includes two metals and it is not soluble in water. The proposed approach is a simple, green, and catalyst-free approach under an ambient environment. Apart from these merits, this novel technique allows researchers to choose and design interesting

* Address correspondence to stsygw@mail.sysu.edu.cn.

Received for review February 22, 2011 and accepted May 24, 2011.

Published online May 25, 2011
10.1021/nn2007282

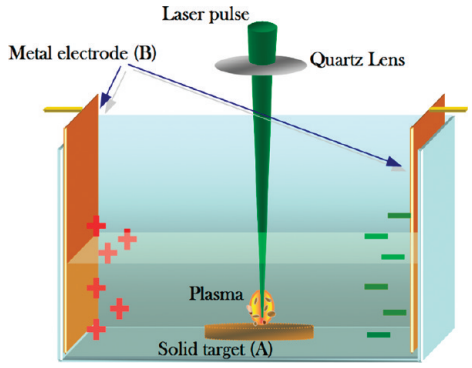

Figure 1. Schematic illustration of electrochemistry-assisted laser ablation in liquid.

solid targets and to use electrochemistry to fabricate POM nanostructures for the purpose of fundamental research and for potential applications. Laser ablation of a solid target in a liquid environment has been widely used in the synthesis of nanocrystals and for the fabrication of nanostructures,[15−28] and it is increasingly recognized to be a general and effective technique.[29−42] Among the many POM materials, the molybdenum oxide-based materials and the copper-containing compounds that consist of mixed metal oxides containing molybdenum and copper species have attracted particular interest in various research fields because of their catalytic properties and, therefore, possible applications in solid-state chemistry, ion exchange, and smart windows.[43−45] Therefore, we use the synthesis of the $Cu_3Mo_2O_9$ nanostructure as an example to show that ECLAL is an effective technique for the synthesis of simple POM nanostructures.

ECLAL generally has three advantages, as shown in Figure 1: (i) it is a chemically "simple and clean" synthesis because of the simple starting materials, no catalyst requirement, and reduced byproduct formation *etc*; (ii) an ambient environment is used without extreme temperature and pressure conditions; (iii) researchers can design nanostructures by combining interesting solid targets (*e.g.*, metals and semiconductors, *etc.*), electrodes, and a mother solution (not only water but also organic liquids or another reactive solution that contains interesting ions) in an electrochemical reaction associated with LAL for fundamental research and for potential applications.

RESULTS AND DISCUSSION

$Cu_3(OH)_2(MoO_4)_2$ Nanorod Synthesis. Typical SEM images of the as-synthesized nanostructures are shown in Figure 2. Clearly, these nanorods are uniform, and their average length is about 3 μm with an average diameter of about 100 nm. Interestingly, the high-magnification SEM image indicates that these rod-like nanostructures have a rough surface and the two tips are not smooth but have defects, as shown by the detailed feature of the single nanorod in the inset of Figure 2a. The

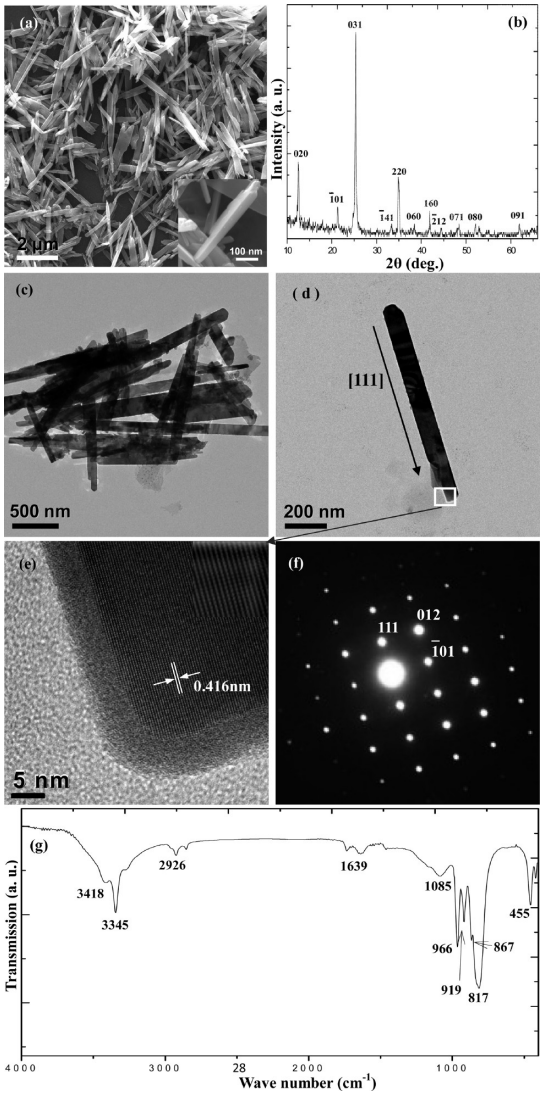

Figure 2. SEM images of the fabricated $Cu_3(OH)_2(MoO_4)_2$ nanorods (a), the corresponding XRD pattern (b), the corresponding TEM bright-field images (c,d), the high-resolution TEM (HRTEM) image of the tip of a nanorod (e), and the corresponding selected area electronic diffraction (SAED) pattern (f). FTIR spectrum of the sample (g).

corresponding XRD pattern of the sample (Figure 2b) shows that the fabricated nanostructure is a pure monoclinic phase of crystalline $Cu_3(OH)_2(MoO_4)_2$. All of the XRD peaks correspond to that in the XRD JCPDS Card File No. 862311. Since there are no diffraction peaks of amorphous molybdenum, copper compounds, or other oxide phase in the XRD pattern, the synthesized sample is highly pure and crystalline. Furthermore, TEM data show the detailed crystalline structure of the $Cu_3(OH)_2(MoO_4)_2$ nanorods, and this is shown in Figure 2e,f. The interplanar spacing of the sample was found to be 0.416 nm, which corresponds well to the *d* value of the $(\bar{1}01)$ crystallographic planes of $Cu_3(OH)_2(MoO_4)_2$ with a monoclinic structure. The corresponding selected area electronic diffraction (SAED) pattern shows the same result. Additionally,

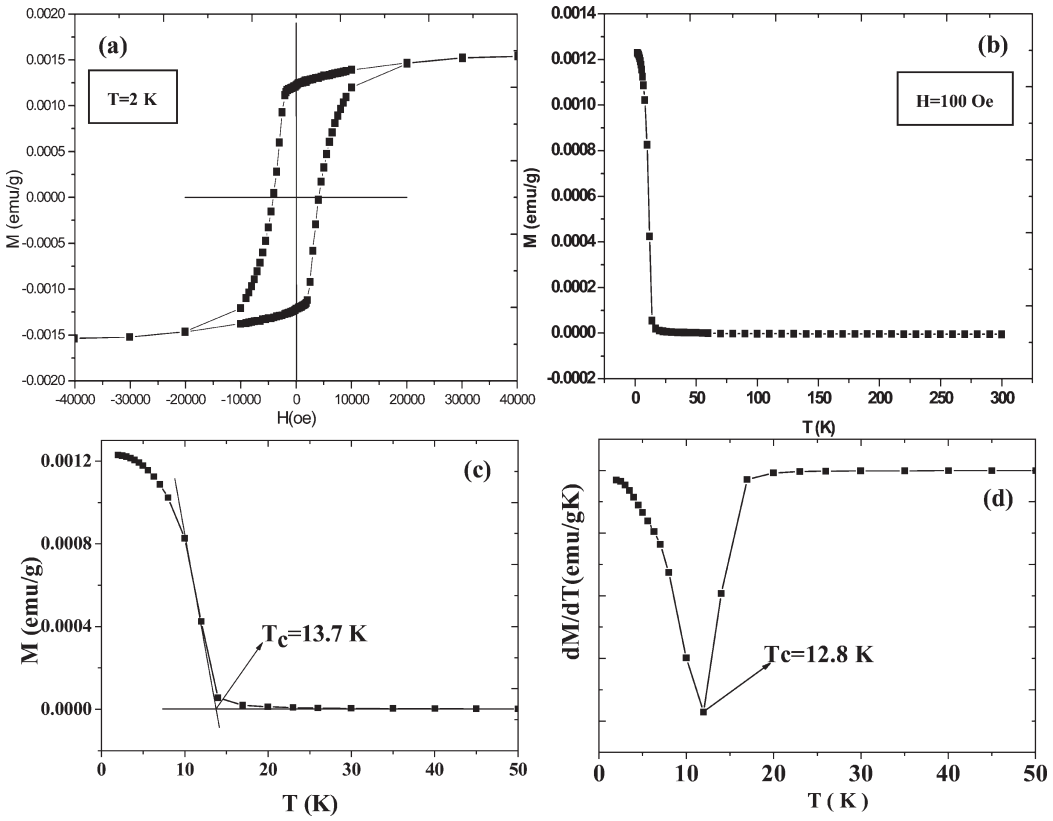

Figure 3. (a) Isothermal magnetization analysis operated at 2 K, and (b) temperature dependence of the dc magnetic susceptibility of $Cu_3(OH)_2(MoO_4)_2$ nanorods. (c) Sketch map of methods of linear extrapolation in achieving Curie temperature (T_C) point of the $Cu_3(OH)_2(MoO_4)_2$ nanorods, and (d) illustration of $M-T$ differential coefficient method in obtaining Curie temperature of the sample.

high-resolution TEM (HRTEM) and SAED reveal that the $Cu_3(OH)_2(MoO_4)_2$ nanorods are elongated along the [111] direction. Finally, FTIR data provide the chemical structure of the sample, as shown in Figure 2g, and 10 IR absorption bands at 455, 817, 867, 919, 966, 1085, 1639, 2926, 3345, and 3418 cm^{-1} were found. Specifically, the band at 455 cm^{-1} can be attributed to the Cu−OH vibration bands of lindgrenite, and the four bands (two sharp, one broad, and one shoulder) located between 817 and 966 cm^{-1} are due to the symmetric vibration bands of the $\nu_3MoO_4^{2-}$ (817, 867, and 919 cm^{-1}) and $\nu_1MoO_4^{2-}$ (966 cm^{-1}) modes of the molybdate ion.[13,46] The band at 1085 cm^{-1} is an antisymmetric absorption peak from the SiO_2 substrate, and the bands at 1639 and 2926 cm^{-1} are proposed to be the infrared active vibrations of the H_2O that is absorbed on the sample.[47,48] The bands at 3345 and 3418 cm^{-1} both correspond to the symmetric and antisymmetric stretching modes of the O−H bonds in $Cu_3(OH)_2(MoO_4)_2$.[13,46] Therefore, FTIR data further confirm that the synthesized nanorods are $Cu_3(OH)_2(MoO_4)_2$.

Magnetic Properties of $Cu_3(OH)_2(MoO_4)_2$ Nanorods. Figure 3 shows the isothermal magnetization *versus* the applied field recorded at 2 K and the temperature dependence of the dc magnetic susceptibility of the sample. The field-dependent magnetization curve recorded at 2 K (Figure 3a) reveals a nonlinear evolution of the fraction with a saturation value at 20 kOe, which indicates that the sample has a ferrimagnetic property. Interestingly, a narrow square shape hysteresis loop was present with a maximum coercive field around 4192 Oe between −20 and +20 kOe. Therefore, these results show how magnetic moments on the carriers are ordered in the $Cu_3(OH)_2(MoO_4)_2$ nanorods at very low temperatures.[46,49] Additionally, the magnetic susceptibility measured in an applied field of 100 Oe was carried out from 300 to 30 K, and the temperature-dependent curve is shown in Figure 3b. The curve decreases gradually from 300 to 25 K in a shallow minimum before a sharp increase. From these data, we can calculate the two Curie temperature points of the sample, and these were 13.7 K as shown in Figure 3c and 12.8 K as shown in Figure 3d. Considering the measurement error, the average of 13.2 K was taken as the Curie temperature of the sample.

$Cu_3Mo_2O_9$ Nanorods Synthesis. Upon annealing the sample at 500 °C for 5 h, the phase transformation from lindgrenite to tertiary copper molybdate ($Cu_3Mo_2O_9$) was achieved as follows:

$$Cu_3(OH)_2(MoO_4)_2 \rightarrow Cu_3Mo_2O_9 + H_2O\uparrow \quad (1)$$

Figure 4 shows the morphology and structure of the $Cu_3Mo_2O_9$ nanostructures. Compared with the

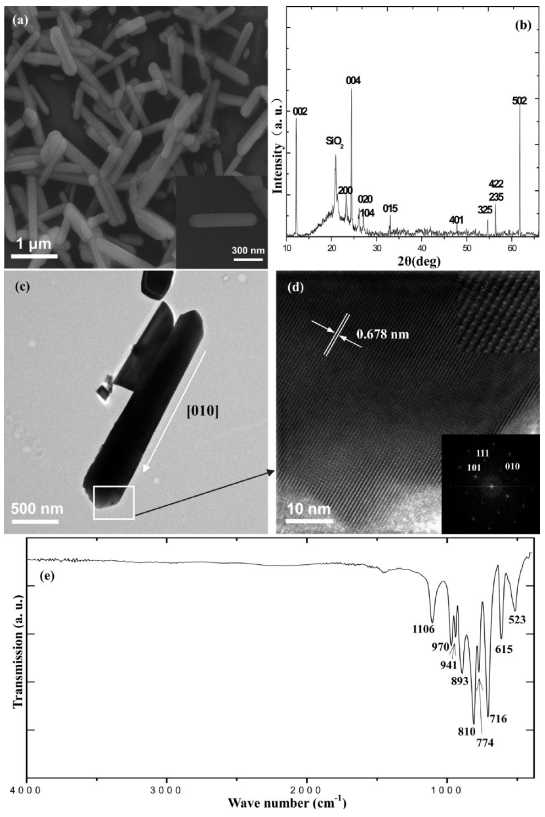

Figure 4. SEM image of the $Cu_3Mo_2O_9$ nanorods (a), the corresponding XRD pattern (b), TEM bright-field image of the sample (c), and the corresponding HRTEM image (d). The clear-cut crystal lattice and a corresponding fast Fourier transform (FFT) analysis are shown in the inset of (d).

$Cu_3(OH)_2(MoO_4)_2$ nanorods, the $Cu_3Mo_2O_9$ nanorods are well-defined and more uniform. Additionally, the average lengths of the $Cu_3Mo_2O_9$ nanorods are shorter, and the average diameter is larger than that of the $Cu_3(OH)_2(MoO_4)_2$ nanorods. The corresponding XRD pattern of the $Cu_3Mo_2O_9$ nanorods shows that almost all of the detected peaks can be indexed to the pure orthorhombic phase of the $Cu_3Mo_2O_9$ crystal (according to XRD JCPDS Card File No. 870455). The peak at 22.31 °C is supposed to originate from the SiO_2 substrate. Furthermore, TEM data reveal the detailed crystalline structure of the $Cu_3Mo_2O_9$ nanorods as shown in Figure 4c,d. The interplanar spacing of the sample was found to be 0.678 nm, which agrees well with the *d* value of the (101) crystallographic planes from the $Cu_3Mo_2O_9$ crystal with an orthorhombic structure. A corresponding fast Fourier transform (FFT) analysis (inset in Figure 4d) of the lattice structure was obtained, and a careful measurement of the indices shows that the lattice fringe directions are the (101) and (010) planes of $Cu_3Mo_2O_9$. Moreover, HRTEM characterization also reveals that the $Cu_3Mo_2O_9$ nanorods are elongated along the [010] direction of the orthorhombic structure, as shown in Figure 4c.

Finally, the FTIR data reveal that the chemical structure of the sample is as shown in Figure 4e, and nine IR absorption bands at 523, 615, 716, 774, 810, 893, 941, 970, and 1106 cm^{-1} are clearly present. A detailed comparison of the aforementioned FTIR data of the $Cu_3(OH)_2(MoO_4)_2$ nanorods is shown in Figure 4e, which shows obvious differences. First, no absorption bands are present that correspond to the symmetric and antisymmetric stretching modes of the O−H peak and the infrared active vibration bands of the H_2O molecule from 1600 to 3900 cm^{-1}.[13,46] This result indicates that there are no hydroxy components present in the prepared sample because of the loss of H_2O during thermal decomposition, as described in eq 1. Second, on the basis of previous research,[50] three new bands at 523, 716, and 774 cm^{-1} (which do not appear in Figure 2g) are shown in Figure 3e, and they are assigned to the antisymmetric absorption peak and to the two symmetric vibration bands of the Cu−O pyramidal structure, which is present in the $Cu_3Mo_2O_9$ crystal.[50] Third, as indicated by Nakamoto, the symmetric vibration bands of the $\nu_1MoO_4^{2-}$ (966 cm^{-1}) and $\nu_3MoO_4^{2-}$ (817, 867, and 919 cm^{-1}) modes of the molybdate ion will shift to a new value when symmetry breaking takes place in the lindgrenite crystal structure. This behavior can be attributed to thermal dehydration upon a phase transformation to the $Cu_3Mo_2O_9$ crystalline structure.[51] Therefore, in our case, the absorption bands at 810, 893, and 941 cm^{-1} can undoubtedly be indexed to the shift modes of the original $\nu_3MoO_4^{2-}$ vibration bands, while that at 970 cm^{-1} can be indexed to a shift mode of the original $\nu_1MoO_4^{2-}$ vibration bands of the $Cu_3Mo_2O_9$ nanocrystal.[51] Additionally, the 615 and 1106 cm^{-1} vibration peaks can be assigned to the Si crystal structure and SiO_2 components, which all come from the Si substrate.[47,48,52] Therefore, FTIR data further confirm that the synthesized nanorods are $Cu_3Mo_2O_9$.

Fabrication Mechanism. Now we discuss the basic physics and chemistry involved in the synthesis of the $Cu_3(OH)_2(MoO_4)_2$ nanorods upon ECLAL. Nanostructure formation upon ECLAL can be divided into three processes as follows: (i) laser ablation in the liquid wherein a plasma plume is generated at the interface between the liquid and solid because of laser ablation of the solid target,[53,54] which contains many Mo ions and other species under high temperature, high density, and high pressure conditions. The deionized water around the plasma plume is ionized to the H^+, OH^-, and O^{2-} species,[55,56] and these active species can combine with the active Mo species in the plasma plume to form a molybdenum oxide species (MoO_3 or even MoO_4^{2-} ions). (ii) An electrochemical reaction, wherein the copper anode is electrolyzed at a suitable voltage causing the Cu^{2+} ions to easily dissolve into the liquid environment, takes place as follows:

$$Cu + 2H_2O \rightarrow Cu(OH)_2 + H_2 \qquad (2)$$

At the same time, the deionized water around the electrode can also be electrolyzed into H and O ions

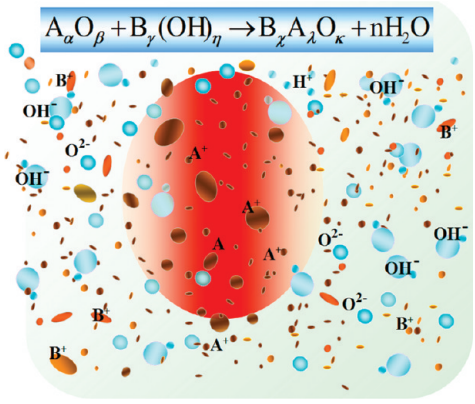

Figure 5. Schematic illustration of fabrication mechanism of nanostructures upon electrochemistry-assisted laser ablation in liquid.

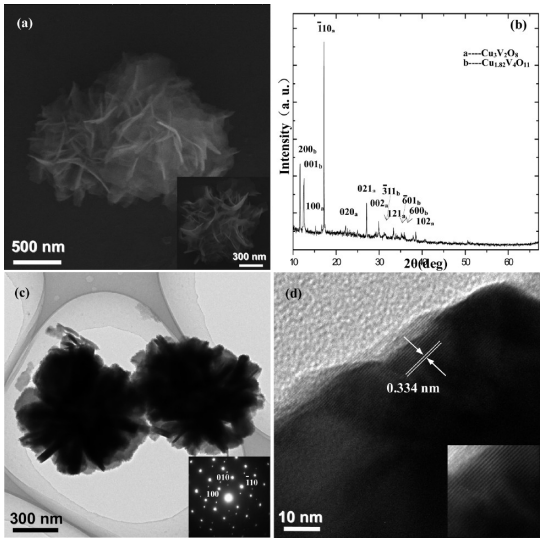

Figure 6. SEM image of the $CuVO_7$ nanoflowers (a), the corresponding XRD pattern (b), TEM bright-field image of the sample (c), and a corresponding SAED analysis is shown in the inset of (c). HRTEM image of one tip of the nanoflower (d).

under the applied electric field conditions, while the active O will surround the plasma and take part in the reaction. (iii) For the nanostructure fabrication, the electric field effect causes the Cu^{2+} ions to show electrophoresis behavior in solution, and this results in the Cu species (Cu^{2+} ions or $Cu(OH)_2$) moving into the plasma plume and reacting with the highly active Mo-containing species (*e.g.*, MoO_3 or MoO_4^{2-}).[57] Furthermore, the incident laser pulses affect the highly active Mo-containing species and causes them to combine with the Cu clusters.[58] Considering the complexity of this reaction, we give a typical equation for this reaction:

$$2MoO_3 + 3Cu(OH)_2 \rightarrow Cu_3(OH)_2(MoO_4)_2 + 2H_2O \quad (3)$$

As a result of high-temperature plasma region induction, the reaction above is very effective.[59] Moreover, in this pathway, the adjacent reactant species combine by sharing a common crystallographic orientation and growth into a morphology that reduces the overall surface energy.[60−62] Additionally, the growth of $Cu_3(OH)_2(MoO_4)_2$ nanorods upon ECLAL is due to oriented attachment with the assistance of the electric field; that is, the stick-like shape of the $Cu_3(OH)_2(MoO_4)_2$ nanostructures originates from the interaction between laser ablation and the electrochemical reaction. A schematic illustration of the fabrication mechanism of the nanostructures upon ECLAL is shown in Figure 5.

As stated above, the generality of the proposed strategy for the fabrication of these polyoxometalate nanostructures is that this novel technique allows researchers to choose and design interesting solid targets and use an electrochemical approach toward the fabrication of nanostructures of polyoxometalate compounds for the purpose of fundamental research and potential applications. Therefore, this synthesis of $Cu_3Mo_2O_9$ nanorods demonstrates our approach. We provide new experiments below to further confirm the conclusions from this work.

From ECLAL, we obtain $Cu_3V_2O_8$ if we replace molybdenum with vanadium during the ECLAL synthesis. In our ECLAL synthesis, the molybdenum target was replaced by a vanadium target (99.97% purity). Interestingly, we successfully synthesized copper vanadate nanostructures, as shown in Figure 6. As shown in Figure 6a, a typical SEM image of the sample indicates that the synthesized nanostructures are flower-like and their average diameter is about 700 nm. This morphology is similar to that reported recently for copper vanadate micro- and nanocrystals synthesized by a hydrothermal technique.[63] The corresponding XRD pattern of the sample was measured as shown in Figure 6b. Upon careful analysis, we found that two phases of the copper vanadate crystal exist in the fabricated nanostructure. The major phase was identified as crystalline $Cu_3V_2O_8$ with a monoclinic structure, while the main diffraction peaks (indexed as a) correspond with XRD JCPDS Card File No. 260567. The other diffraction peaks are assigned to the monoclinic structure of the $Cu_{1.82}V_4O_{11}$ crystal (indexed as b), which can be indexed to XRD JCPDS Card File No. 260567. Furthermore, the TEM data in Figure 6c,d show the detailed crystalline structure of the sample. The bright-field TEM image of the synthesized nanostructure shows that these nanoflowers consist of many sheet-like nanofittings, and the corresponding SAED pattern (shown in the inset) can be indexed exactly to the (100), ($\bar{1}$10), and (010) planes of the $Cu_3V_2O_8$ crystal. Conversely, the HRTEM analysis in Figure 6d shows that the interplanar spacing of the sample was 0.334 nm, which corresponds well to the *d* value of the (021) crystallographic planes of crystalline $Cu_3V_2O_8$ with a monoclinic structure.

Therefore, all of the experimental data discussed above confirm that we could choose and design interesting solid targets and use an electrochemical

approach to fabricate nanostructures of simple POM compounds.

CONCLUSIONS

In summary, we propose a general strategy for the fabrication of specific and simple POM nanostructures by electrochemically assisted laser ablation in liquid. This technique is a simple, green, and catalyst-free approach under an ambient environment. Apart from these merits, this novel approach allows researchers to choose and design interesting solid targets and to use electrochemistry to fabricate nanostructures of POM compounds for the purpose of fundamental research and potential applications. Using the synthesis of $Cu_3Mo_2O_9$ nanorods as an example, we showed the validity of the proposed strategy. For the fabrication of $Cu_3Mo_2O_9$ nanostructures, we chose molybdenum as a solid target for the laser ablation in liquid, and we used copper electrodes for the electrochemical reaction in ECLAL. As a result, we successfully fabricated $Cu_3(OH)_2(MoO_4)_2$ nanorods with magnetic properties. Interestingly, well-defined $Cu_3Mo_2O_9$ nanorods were obtained in a facile manner by annealing the $Cu_3(OH)_2(MoO_4)_2$ products at 500 °C. The basic physics and chemistry involved in the ECLAL fabrication of the nanostructures are discussed.

METHODS

For the fabrication of the $Cu_3Mo_2O_9$ nanostructure in the ECLAL synthesis, we chose molybdenum (99.95% purity) as a solid target, copper (99.99% purity) electrodes, and deionized water as the solvent. The Mo target was initially attached to the bottom of a rectangular quartz chamber. Deionized water was then poured slowly into the chamber until the target was covered with 10 mm. Then, two Cu electrodes were placed between the two sides of the chamber. The distance between the two electrodes was 50 mm. A steady electric field with an adjusted voltage of 20 V was produced by a direct current voltage power source. The second harmonic laser was produced by a Q-switched Nd:YAG laser device with a wavelength of 532 nm, a repeating frequency of 5 Hz, a pulse width of 10 ns, and a pulse energy of 100 mJ/pulse. Finally, the pulsed laser was focused onto the surface of the Mo target. During laser ablation, the target and liquid environment were both maintained at room temperature. After the whole interaction, which lasted for 60 min, the mother solution was evaporated and collected on silicon substrates for further measurements. Scanning electron microscopy (SEM), X-ray diffraction analysis (XRD), transmission electron microscopy (TEM), and Fourier transform infrared spectroscopy (FTIR) were used to identify the morphology, composition, and structure of the synthesized samples and a Quantum Design MPMS-XL7 SQUID magnetometer was used to measure the magnetic susceptibility of the samples upon cooling from 300 to 2 K in a 0.010 T applied field.

Acknowledgment. NSFC (U0734004 and 11004253), the China Postdoctoral Science Foundation (20090460830), and the Ministry of Education supported this work.

REFERENCES AND NOTES

1. Hill, C. L.; KIM, G. S.; Prosser-Mccartha, C. M.; Judd, A. D. Polyoxometalates in Catalytic Selective Homogeneous Oxygenation and Anti-HIV Chemotherapy. *Mol. Eng.* **1993**, *3*, 263–275.
2. Coronado, E.; Gomez-Garcia, C. J. Polyoxometalate-Based Molecular Materials. *Chem. Rev.* **1998**, *98*, 273–296.
3. Long, D. L.; Burkholder, E.; Cronin, L. Polyoxometalate Clusters, Nanostructures and Materials: From Self Assembly to Designer Materials and Devices. *Chem. Soc. Rev.* **2007**, *36*, 105–121.
4. Song, C. S.; Ma, X. L. New Design Approaches to Ultra-clean Diesel Fuels by Deep Desulfurization and Deep Dearomatization. *Appl. Catal., B* **2002**, *41*, 207–238.
5. Ivanov, A.; Dimitrov, D.; Boyanov, B. Optimization of the Methanol Oxidation over Iron−Molybdate Catalysts. *Chem. Eng. J.* **2009**, *154*, 189–195.
6. Wang, Q. M.; Yan, B. Hydrothermal Mild Synthesis of Microrod Crystalline $Y_xGd_{2-x}(MoO_4)_3$:Eu^{3+} Phosphors Derived from Facile Co-precipitation Precursors. *Mater. Chem. Phys.* **2005**, *94*, 241–244.
7. Yu, S.; Lin, Z. B.; Zhang, L. Z.; Wang, G. F. Preparation of Monodispersed Eu^{3+}:$CaMoO_4$ Nanocrystals with Single Quasihexagon. *Cryst. Growth. Des.* **2007**, *7*, 2397.
8. Tripathy, D.; Adeyeye, A. O.; Boothroyd, C. B.; Piramanayagam, S. N. Magnetic and Transport Properties of Co-doped Fe_3O_4 Films. *Appl. Phys. Lett.* **2007**, *101*, 013904.
9. Xu, J.; Xue, D. Room Temperature Synthesis of Curved Ammonium Copper Molybdate Nanoflake and Its Hierarchical Architecture. *J. Phys. Chem. B* **2006**, *110*, 17400–17405.
10. Kim, S. S.; Ogura, S.; Ikuta, H.; Uchimoto, Y.; Wakihara, M. Reaction Mechanisms of $MnMoO_4$ for High Capacity Anode Material of Li Secondary Battery. *Solid State Ionics* **2002**, *146*, 249–256.
11. Chu, W. G.; Wang, H. F.; Guo, Y. J.; Zhang, L. N.; Han, Z. H.; Li, Q. Q.; Fang, S. S. Catalyst-Free Growth of Quasi-aligned Nanorods of Single Crystal $Cu_3Mo_2O_9$ and Their Catalytic Properties. *Inorg. Chem.* **2009**, *48*, 1243–1249.
12. Breysse, M.; Geantet, C.; Afanasiev, P.; Blanchard, J.; Vrinat, M. Recent Studies on the Preparation, Activation and Design of Active Phases and Supports of Hydrotreating Catalysts. *Catal. Today* **2008**, *130*, 3–13.
13. Xu, J. S.; Xue, D. F. Hydrothermal Synthesis of Lindgrenite with a Hollow and Prickly Sphere-like Architecture. *J. Solid State Mater.* **2006**, *180*, 119–126.
14. Canevali, C.; Morazzoni, F.; Scotti, R.; Cauzzi, D.; Moggi, P.; Predieri, G. Electron Paramagnetic Resonance Characterisation of Silica-Dispersed Copper Molybdate Obtained by Sol−Gel and Impregnation Methods. *J. Mater. Chem.* **1999**, *9*, 507–513.
15. Yang, G. W.; Wang, J. B.; Liu, Q. X. Preparation of Nanocrystalline Diamonds Using Pulsed Laser Induced Reactive Quenching. *J. Phys.: Condens. Matter* **1998**, *10*, 7923–7927.
16. Mafune, F.; Kohno, J.; Takeda, Y.; Kondow, T. Full Physical Preparation of Size-Selected Gold Nanoparticles in Solution: Laser Ablation and Laser-Induced Size Control. *J. Phys. Chem. B* **2002**, *106*, 7575–7577.
17. Wang, J. B.; Yang, G. W.; Zhang, C. Y.; Zhong, X. L.; Ren, Zh. A. Cubic-BN Nanocrystals Synthesis by Pulsed Laser Induced Liquid−Solid Interfacial Reaction. *Chem. Phys. Lett.* **2003**, *367*, 10–14.
18. Mafune, F.; Kohno, J.; Takeda, Y.; Kondow, T. Formation of Gold Nanonetworks and Small Gold Nanoparticles by Irradiation of Intense Pulsed Laser onto Gold Nanoparticles. *J. Phys. Chem. B* **2003**, *107*, 12589–12596.
19. Liu, Q. X.; Wang, C. X.; Zhang, W.; Yang, G. W. Immiscible Silver−Nickel Alloying Nanorods Growth upon Pulsed-Laser Induced Liquid/Solid Interfacial Reaction. *Chem. Phys. Lett.* **2003**, *382*, 1–5.
20. Compagnini, G.; Scalisi, A. A.; Puglisi, O. Synthesis of Gold Colloids by Laser Ablation in Thiol-Alkane Solutions. *J. Mater. Res.* **2004**, *19*, 2795–2798.

21. Liang, C. H.; Shimizu, Y.; Sasaki, T; Koshizaki, N. Preparation of Ultrafine TiO_2 Nanocrystals *via* Pulsed-Laser Ablation of Titanium Metal in Surfactant Solution. *Appl. Phys. A: Mater. Sci. Process.* **2005**, *80*, 819–822.
22. Besner, S.; Kabashin, A. V.; Meunier, M. Two-Step Femtosecond Laser Ablation-based Method for the Synthesis of Stable and Ultra-pure Gold Nanoparticles in water. *Appl. Phys. A* **2007**, *88*, 269–272.
23. Lv, K. M.; Yang, J.; Niu, K. Y.; Wang, H. L.; Sun, J.; Du, X. W. Synthesis of Si-C Nanostructures by Laser Ablation of Silicon Target in *n*-Heptane Vapor. *Mater. Lett.* **2009**, *63*, 2492–2494.
24. Chen, X. Y.; Cui, H.; Liu, P.; Yang, G. W. Double-Layer Hexagonal Fe Nanocrystals and Magnetism. *Chem. Mater.* **2008**, *20*, 2035–2038.
25. Niu, K. Y.; Yang, J.; Kulinich, S. A.; Sun, J.; Li, H.; Du, X. W. Morphology Control of Nanostructures *via* Surface Reaction of Metal Nanodroplets. *J. Am. Chem. Soc.* **2010**, *132*, 9814–9819.
26. Wang, H. Q.; Pyatenko, A.; Kawaguchi, K.; Li, X. Y.; Warkocka, Z. S.; Koshizaki, N. Selective Pulsed Heating for the Synthesis of Semiconductor and Metal Submicrometer Spheres. *Angew. Chem., Int. Ed.* **2010**, *49*, 6361–6364.
27. Mhin, S. W.; Ryu, J. H.; Kim, K. M.; Park, G. S.; Ryu, H. W.; Shim, K. B.; Sasaki, T.; Koshizaki, N. Simple Synthetic Route for Hydroxyapatite Colloidal Nanoparticles *via* a Nd:YAG Laser Ablation in Liquid Medium. *Appl. Phys. A* **2009**, *96*, 435–440.
28. Amendola, V.; Meneghetti, M. Laser Ablation Synthesis in Solution and Size Manipulation of Noble Metal Nanoparticles. *Phys. Chem. Chem. Phys.* **2009**, *11*, 3805–3821.
29. He, C.; Sasaki, T.; Zhou, Y.; Shimizu, Y.; Masuda, M.; Koshizaki, N. Surfactant-Assisted Preparation of Novel Layered Silver Bromide-Based Inorganic/Organic Nanosheets by Pulsed Laser Ablation in Aqueous Media. *Adv. Funct. Mater.* **2007**, *17*, 3554–3561.
30. Compagnini, G.; Messina, E.; Puglisi, O.; Nicolosi, V. Laser Synthesis of Au/Ag Colloidal Nano-alloys: Optical Properties, Structure and Composition. *Appl. Surf. Sci.* **2007**, *254*, 1007–1011.
31. Liu, P.; Cao, Y. L.; Cui, H.; Chen, X. Y.; Yang, G. W. Micro- and Nanocubes of Silicon with Zinc-Blende Structure. *Chem. Mater.* **2008**, *20*, 494–502.
32. Liu, P.; Cui, H.; Yang, G. W. Synthesis of Body-Centered Cubic Carbon Nanocrystals. *Cryst. Growth Des.* **2008**, *8*, 581–586.
33. Besner, S.; Kabashin, A. V.; Winnik, F. M.; Meunier, M. Ultrafast Laser Based "Green" Synthesis of Non-toxic Nanoparticles in Aqueous Solutions. *Appl. Phys. A* **2008**, *93*, 955–959.
34. Liu, P.; Cao, Y. L; Wang, C. X.; Chen, X. Y.; Yang, G. W. Micro- and Nanocubes of Carbon with C_8-like and Blue Luminescence. *Nano Lett.* **2008**, *8*, 2570–2575.
35. Liu, P.; Wang, C. X.; Chen, J.; Xu, N. S.; Yang, G. W.; Ke, N.; Wang, J. B. Localized Nanodiamond Crystallization and Field Emission Performance Improvement of Amorphous Carbon upon Laser Irradiation in Liquid. *J. Phys. Chem. C* **2009**, *113*, 12154–12161.
36. Liu, P.; Cao, Y. L.; Chen, X. Y.; Yang, G. W. Trapping High-Pressure Nanophase of Ge upon Laser Ablation in Liquid. *Cryst. Growth Des.* **2009**, *9*, 1390–1393.
37. Zeng, H. B.; Li, Z. G.; Cai, W. P.; Cao, B. Q.; Liu, P. S.; Yang, S. K. Microstructure Control of Zn/ZnO Core/Shell Nanoparticles and Their Temperature-Dependent Blue Emissions. *J. Phys. Chem. B* **2007**, *111*, 14311–14317.
38. Du, X. W.; Qiu, W. J.; Lu, Y. W.; Han, X.; Fu, Y. S.; Hu, S. L. Face-Centered-Cubic Si Nanocrystals Prepared by Microsecond Pulsed Laser Ablation. *J. Appl. Phys.* **2007**, *102*, 013518.
39. Sasaki, T.; Shimizu, Y.; Koshizaki, N. Preparation of Metal Oxide-Based Nanomaterials Using Nanosecond Pulsed Laser Ablation in Liquids. *J. Photochem. Photobiol. A* **2006**, *182*, 335–341.
40. Chen, X. Y.; Cui, H.; Liu, P.; Yang, G. W. Shape-Induced Ultraviolet Absorption of CuO Shuttlelike Nanoparticles. *Appl. Phys. Lett.* **2007**, *90*, 183118.
41. Liu, P.; Cao, Y. L.; Cui, H.; Chen, X. Y.; Yang, G. W. Synthesis of GaN Nanocrystals through Phase Transition from Hexagonal to Cubic Structures upon Laser Ablation in Liquid. *Cryst. Growth Des.* **2008**, *8*, 559–563.
42. Liu, P.; Cui, H.; Wang, C. X.; Yang, G. W. From Nanocrystal Synthesis to Functional Nanostructure Fabrication: Laser Ablation in Liquid. *Phys. Chem. Chem. Phys.* **2010**, *12*, 3942–3952.
43. Liu, H. W.; Tan, L. Synthesis, Structure, and Electrochemical Properties of $CdMoO_4$ Nanorods. *Ionics* **2010**, *16*, 57–60.
44. Ozin, G. A.; Ozkar, S.; Prokopowicz, R. A. Smart Zeolites: New Forms of Tungsten and Molybdenum Oxide. *Acc. Chem. Res.* **1992**, *25*, 553–560.
45. Hamelmann, F.; Gesheva, K.; Ivanova, T.; Szekeres, A.; Abroshev, M.; Heinzmann, U. Optical and Electrochromic Characterization of Multilayered Mixed Metal Oxide Thin Films. *J. Optoelectron. Adv. Mater.* **2005**, *7*, 393–396.
46. Vilminot, S.; Andre, G.; Richard-Plouet, M.; Bouree-Vigneron, F.; Kurmoo, M. Magnetic Structure and Magnetic Properties of Synthetic Lindgrenite, $Cu_3(OH)_2(MoO_4)_2$. *Inorg. Chem.* **2006**, *45*, 10938–10946.
47. Hofman, R.; Westheim, J. G. F.; Pouwel, I.; Fransen, T.; Gellings, P. J. FTIR and XPS Studies on Corrosion-Resistant SiO_2 Coatings as a Function of the Humidity during Deposition. *Surf. Interface Anal.* **1996**, *24*, 1–6.
48. Zhang, Y. P.; Lee, S. H.; Reddy, K. R.; Gopalan, A. I.; Lee, K. P. Synthesis and Characterization of Core−Shell SiO_2 Nanoparticles/Poly(3-aminophenylboronic acid) Composites. *J. Appl. Polym. Sci.* **2007**, *104*, 2743–2750.
49. Shores, M. P.; Barelett, B. M.; Nocera, D. G. Spin-Frustrated Organic−Inorganic Hybrids of Lindgrenite. *J. Am. Chem. Soc.* **2005**, *127*, 17986–17987.
50. Vilminot, S.; Andre, G.; Kurmoo, M. Magnetic Properties and Magnetic Structure of $Cu^{II}_3Mo^{VI}_2O_9$. *Inorg. Chem.* **2009**, *48*, 2687–2692.
51. Nakamoto, K. *Infrared and Raman Spectra of Inorganic and Coordination Compounds*, 4th ed.; John Wiley & Sons: New York, 1986.
52. Chen, S. Y.; Xie, S.; He, G. R. FTIR and XPS Analysis of Directly Bonded Si/Si Interface. *Semicond. Optoelectron.* **2004**, *25*, 372–375.
53. Yang, G. W. Laser Ablation in Liquids: Applications in the Synthesis of Nanocrystals. *Prog. Mater. Sci.* **2007**, *52*, 648–698.
54. Wang, C. X.; Liu, P.; Cui, H.; Yang, G. W. Nucleation and Growth Kinetics of Nanocrystals Formed upon Pulsed-Laser Ablation in Liquid. *Appl. Phys. Lett.* **2005**, *87*, 201913.
55. Sakka, T.; Iwanaga, S.; Ogata, Y. H.; Matsunawa, A.; Takemoto, T. Laser Ablation at Solid−Liquid Interfaces: An Approach from Optical Emission Spectra. *J. Chem. Phys.* **2000**, *112*, 8645–8653.
56. Liang, C. H.; Sasaki, T.; Shimizu, Y.; Koshizaki, N. Pulsed-Laser Ablation of Mg in Liquids: Surfactant-Directing Nanoparticle Assembly for Magnesium Hydroxide Nanostructures. *Chem. Phys. Lett.* **2004**, *389*, 58–63.
57. Oliveira, J. A.; De Almeida, W. B.; Duarte, H. D. Density Functional Study of the Mo_xO_y and Mo_xOy^+ ($x = 1-3$; $y = 1-9$) Oxide Clusters. *Chem. Phys. Lett.* **2003**, *372*, 650–658.
58. Aubriet, F.; Muller, J. F. About the Atypical Behavior of CrO_3, MoO_3, and WO_3 during Their UV Laser Ablation/Ionization. *J. Phys. Chem. A* **2002**, *106*, 6053–6059.
59. Liu, P.; Wang, C. X.; Chen, X. Y.; Yang, G. W. Controllable Fabrication and Cathodoluminescence Performance of High-Index Facets GeO_2 Micro- and Nanocubes and Spindles upon Electrical-Field-Assisted Laser Ablation in Liquid. *J. Phys. Chem. C* **2008**, *112*, 13450–13456.
60. Xu, H. L.; Wang, W. Z.; Zhu, W.; Zhou, L.; Ruan, M. L. Hierarchical-Oriented Attachment: From One-Dimensional $Cu(OH)_2$ Nanowires to Two-Dimensional CuO Nanoleaves. *Cryst. Growth. Des.* **2007**, *7*, 2720–2724.
61. Godinho, M.; Ribeiro, C.; Longo, E.; Leite, E. R. Influence of Microwave Heating on the Growth of Gadolinium-Doped Cerium Oxide Nanorods. *Cryst. Growth. Des.* **2008**, *8*, 384–386.

62. Wang, J.; He, S. S.; Li, Z. S.; Jing, X. Y.; Zhang, M. L.; Jiang, Z. H. Self-Assembled CuO Nanoarchitectures and Their Catalytic Activity in the Thermal Decomposition of Ammonium Perchlorate. *Colloid Polym. Sci.* **2009**, *287*, 853–858.
63. Sun, X. J.; Wang, J. W.; Xing, Y.; Zhao, Y.; Liu, X. C.; Liu, B.; Hou, S. Y. Surfactant-Assisted Hydrothermal Synthesis and Electrochemical Properties of Nanoplate-Assembled 3D Flower-like $Cu_3V_2O_7(OH)_2 \cdot 2H_2O$ Microstructures. *CrystEngComm* **2011**, *13*, 367–370.